Photosynth Res (2012) 111:205–217
DOI 10.1007/s11120-011-9665-x

REVIEW

Neutron and light scattering studies of light-harvesting photosynthetic antenna complexes

Kuo-Hsiang Tang · Robert E. Blankenship

Received: 21 December 2010 / Accepted: 2 June 2011 / Published online: 28 June 2011

Abstract Small-angle neutron scattering (SANS) and dynamic light scattering (DLS) have been employed in studying the structural information of various biological systems, particularly in systems without high-resolution structural information available. In this report, we briefly present some principles and biological applications of neutron scattering and DLS, compare the differences in information that can be obtained with small-angle X-ray scattering (SAXS), and then report recent studies of SANS and DLS, together with other biophysical approaches, for light-harvesting antenna complexes and reaction centers of purple and green phototrophic bacteria.

Keywords Chlorosomes · *Chloroflexus aurantiacus* · Dynamic light scattering · Light-harvesting antennas · Small-angle neutron scattering · Purple bacteria · Reaction centers

Neutron scattering

Elastic scattering of radiation from photons (optical or X-rays), neutrons, and electrons have been commonly employed in determining structures of condensed matter over almost one century (Nobel prizes to Max von Laue in 1914 and to William H. Bragg and William L. Bragg in 1915). Some properties of the neutron are: uncharged, mass of 1.0087 atomic mass unit, nuclear spin of ½, magnetic moment of −1.913 nuclear magnetons (μ_N), and a lifetime ~887 s (Chadwick 1932a, b). Neutrons are scattered by nuclei through deep penetration in molecules. In contrast, the photon has a spin of 1 but has neither charge nor magnetic moment, and is scattered by the electron cloud of atoms and molecules (Price and Skold 1986). High-flux neutrons are currently produced by two sources: (1) nuclear fission chain reaction, in which neutrons are generated through collisions of fissile nucleus, mainly U^{235}, with an incident neutron beam, and heavy water (^2H_2O or D_2O) is used as the moderator to slow down the fission neutrons to thermal energies in continuous neutron reactors (Duderstadt and Hamilton, 1976); or (2) spallation nuclear reaction, where neutrons are produced by striking heavy metals (W^{183} or U^{238}) with a high-energy accelerated proton beam in spallation neutron sources, and the generated neutrons are then moderated as in the case of a nuclear reactor. Further, it has been suggested that inertial confinement fusion has the potential to produce orders of magnitude more neutrons than spallation (Taylor et al. 2007). Neutrons in small-angle neutron scattering (SANS) measurements are generated from nuclear fission in high-flux reactors and detected by a 2-dimensional ^{3}He gas area detector, in which absorption or capture of neutrons with ^{3}He gas produce proton and tritium (neutron + ^{3}He → proton + ^{3}H + 0.764 MeV (Crawford 1996). The ^{3}He gas detector only records "yes" or "no" events without a direct measurement of energy.

The total neutron scattering cross-section is contributed from both coherent and incoherent scattering. The cross-section is a measurement of the effective surface of the neutron-nucleus interaction potential. The larger the effective surface is, the stronger the scattering (Price and Skold 1986). Hydrogen is known to have much larger incoherent scattering cross-section (79.8 barns, 1 barn = 10^{-24} cm^2) than the other atoms (for example, ^{2}H

K.-H. Tang · R. E. Blankenship (✉)
Department of Biology and Department of Chemistry, Washington University in St. Louis, Campus Box 1137, St. Louis, MO 63130, USA
e-mail: Blankenship@wustl.edu

Table 1 Some comparisons and practical perspectives for SANS and SAXS measurements

	SANS	SAXS
Incident beam sources	Neutrons	Photons (X-rays)
Interacting field	Nuclei (fluctuations in the nuclear densities of the sample)	Electrons (inhomogeneities in electron densities of the sample)
Incident beam wavelength (Å)	4.0–25.0	1.0–1.5
Incident beam flux (i.e., relative brilliance of source)	Very low to low	Medium to high (in synchrotron sources)
Typical sample counting time	Minutes to hours	Seconds to minutes
Coherent scattering length (10^{-12} cm)	H, −0.374; D, 0.667	H, 0.28; D, 0.28
Scattering length density (10^{10} cm^{-2})	H_2O, −0.5; D_2O, 6.4	H_2O, 9.4; D_2O, 9.4
Incoherent scattering	High	Low
Sample restriction	No	No
Sample volumes required	Large	Small
Contrast variation and ^{2}H-isotope labeling	Commonly used (large contrast variation)	Rarely used (small or no contrast variation)
Structural information for an individual unit in multi-component systems	Yes	No
Radiation/heat damage to sample	No	High (especially in synchrotron radiation)
Sample reused	Yes	No
Resolution (vs. atomic-resolution structures)	Low	Low
Sample amount required	High	Medium
Available facility	Large facility only	Laboratory and synchrotron radiation sources

(deuterium, D), 2.0 barns; ^{12}C and ^{16}O, 0.0 barn (^{13}C, 0.034 barn; ^{17}O, 0.004 barn; ^{18}O, 0.0 barn); ^{14}N, 0.5 barns (^{15}N, 0.00005 barn); ^{31}P, 0.005 barn; and ^{32}S, 0.0 barn) (Rauch and Waschkowski 2000). As the neutron wavelength (∼Å) is equal to the inter-atomic distance and the energy (∼meV) corresponds to the thermal fluctuation, molecular dynamics can be measured by incoherent neutron scattering of hydrogen. It is particularly useful to measure the dynamics of biological molecules, in which hydrogen atoms (and protons) are abundant and wide-spread, with dominant incoherent scattering of hydrogen, whereas the incoherent neutron scattering cross-section for carbon, oxygen, nitrogen, phosphate, and sulfur (other major elements in biological molecules) is negligible (Gabel et al. 2002; Smith 1991).

While hydrogen has a larger incoherent scattering length (25.27×10^{-13} cm) than deuterium (4.04×10^{-13} cm), deuterium has a much larger coherent scattering length (6.67×10^{-13} cm) than hydrogen (-3.74×10^{-13} cm) (see Table 1) (Sears 1986). The origin and detailed information of the neutron scattering length can be found in the literature (Sears 1989; Squires 1997), and the sign convention of neutron scattering length was established by Enrico Fermi in 1947. In contrast, the scattering density of X-rays is proportional to the electron number of the atom (Feigin and Svergun 1987). The differences of coherent neutron scattering length between deuterium and hydrogen make SANS, which is an elastic coherent scattering technique, a useful tool to probe structural information of biomolecules and other types of condensed matter. An analogous technique to SANS that employs X-rays is small-angle X-ray scattering (SAXS).

Small-angle neutron scattering (SANS)

Small-angle scattering (SAS), including SANS and SAXS, probes the statistical ensemble of the macrostructures, and deals with the deviation of electromagnetic or particle waves by heterogeneities in matter. The scattering data of SAS are collected at different sample-to-detector distances and cover the desired q range. q (scattering vector or wave-vector transfer) is the difference of the scattered wave-vector (k') and incident wave-vectors (k). $q = 4\pi\sin\theta/\lambda$, where 2θ is the scattering angle. The angular (q) dependence of the scattering intensity, $I(q)$, can be generally expressed in Eq. 1.

$$I(q) = n\Delta\rho^2 V^2 P(q) S(q) \quad (1)$$

where n is the number density of particles, V is the volume of the particle, $\Delta\rho$ is the difference between the scattering length densities (ρ) of the particle and the solvent (i.e., the contrast factor), $P(q)$ is the form or shape factor that gives information on particle size and shape, and $S(q)$ is the structure factor that describes intermolecular correlations between scattering particles; for dilute solutions

$S(q)$ approaches unity. Furthermore, the normalized form factor $P(q)$ as defined above approaches unity as q approaches zero.

The SAS data of samples are recorded in reciprocal (Fourier) space, like the data collection in X-ray and neutron diffraction, and the size (i.e., the radius of gyration, cross-sectional radius, and longest distance of the particle), shape/morphology (compact, lamellar, or rod-shape) and molecular mass of the particles are extracted from the integral parameters of the scattering data. More structural information can be acquired from direct modeling of the scattering data in the reciprocal space, and/or from the density (probability) distribution profile (i.e., $P(r)$ versus r plot) in real space via indirect Fourier transform of the scattering data in reciprocal space (Glatter 1977; Moore 1980; Svergun et al. 1988). Thus, the way to acquire structural information is different for SAS compared to electron microscopic techniques, such as transmission electron microscopy (TEM), scanning electron microscopy (SEM), and cryo-electron microscopy (cryo-EM), which acquire the structural information in real (direct) space and report image intensity that corresponds to the electron density of the selected portions in the sample, whereas SAS cannot produce an image in real space. Note that EM is applied exclusively on very thin samples and cannot measure samples at different concentrations. In contrast, without the sample drying and freezing required by EM, SAS are non-destructive methods and can acquire structural information on biological samples under near-physiological conditions. Further, SANS can measure samples without concerns of radiation-caused structural damage. Together, EM and SAS are complementary methods.

Because deuterium has a much larger coherent neutron scattering length than hydrogen (see above), deuterium (^{2}H)-isotope labeling and contrast variation have been employed in SANS for probing the structural information of biological molecules. For a multi-component biological system, the structural information of the individual components of multi-component biomolecular complexes can be best probed through selective deuterium labeling, when the scattering of the other unlabeled components is rather weak. Such biological systems can be nucleic acid–protein complexes, multi-protein complexes, protein–carbohydrate complexes, protein–lipid complexes, protein–pigment complexes in photosynthetic apparatus, and others. However, selective deuterium labeling one component of the biological complex is occasionally challenging or even not feasible. Alternatively, the structural information of the individual components of biomolecules can sometimes be probed without performing deuterium-isotopic labeling by varying the D_2O ratio in solution, called contrast variation or scattering length density matching (Jacrot 1976).

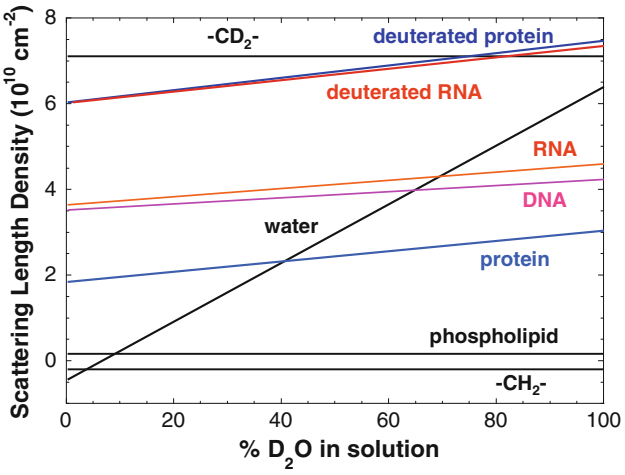

Fig. 1 The profile of scattering length density versus percentage of D_2O in solution. The information is adapted from a report by Jacrot (1976)

The general concept of contrast variation is briefly illustrated as follows: The values of the coherent neutron scattering length densities for H_2O and D_2O are -0.5×10^{10} cm^{-2} and 6.4×10^{10} cm^{-2}, respectively, so the solvent scattering length density is varied by changing the D_2O/H_2O ratio. Similarly, the average scattering length density of the solutes is also varied in different D_2O/H_2O ratios through exchanging labile hydrogen atoms with deuteriums in solution. Scattering length density matching occurs when the average scattering length density (ρ) of the solute is equal to that of the solvent (i.e., $\rho_{solute} = \rho_{solvent}$). The match points for lipids, proteins and nucleic acids are 5–25%, 40–45%, and 65–70% D_2O, respectively (Fig. 1) (Jacrot 1976), so the structural information of the individual components in protein–lipid, protein–polysaccharide, and protein–nucleic acid complexes can be probed in different D_2O/H_2O ratios. The same principle has been used in neutron diffraction and crystallography of protein–lipid complexes (Prince et al. 2003; Roth et al. 1991). Compared to deuterium labeling, scattering length density matching is a convenient approach to acquire structural information in certain biological systems, but often requires (much) higher concentration of samples than deuterium labeling, and this technique is also not useful for probing the structural information of an individual component of multi-protein or multi-nucleic acid complexes. Further, contrast variation has also been applied in SAXS, whereas the application is rather limited compared to SANS (Svergun et al. 1994). In contrast to neutron scattering, the scattering length is the same for H vs. D in X-ray (same number of electrons in H and D) (Table 1), and the X-ray scattering length density of H_2O versus D_2O is also the same (9.4×10^{10} cm^{-2}).

In contrast to diffraction and crystallography, a wide variety of samples, which can be solution, solid, powder, or crystal, can be measured by SANS. Further, because a wide range of wavelengths (4.0–25.0 Å, see Table 1) can be achieved by the use of "cold" (slow) neutron sources, SANS, which uses cold neutrons, can probe particles up to near micron sizes that SAXS, in which the incident X-ray wavelength is limited to usually 1.0–1.5 Å due to absorption restrictions, cannot probe. Thus, SANS has been proved to be a useful tool to probe nanoscale structures in biology. Also, radiation damage is not a concern in neutron scattering. However, in a practical perspective, one of the major drawbacks for SANS is, in contrast to SAXS, that no "in house" SANS instrument is available at this moment and samples must be transported to one of a few centralized facilities. Request for measurement time is generally via a proposal system, in which deadlines are usually twice a year and beamtime, if allocated, is attributed to the users about 6 months later. Also, although SANS has been proved to be a useful tool to obtain structural information for the biological systems without atomic-resolution structures, one needs to note that the major limitation of all solution scattering techniques is the resolution. Another disadvantage for SANS compared to SAXS is that the flux of neutrons is far weaker than that of X-rays, and even the most powerful neutron source in the world is several orders of magnitude weaker than the rotary anode X-ray source in regular laboratories (10^8–10^9 neutrons/cm^2/s vs. $\sim 10^{11}$ X-rays/cm^2/s). Thus, SANS requires larger sample volume and higher sample concentration at certain contrast points, as well as longer measurement time, to acquire useful scattering signals compared to SAXS. In general, SAXS has normally higher signal versus noise (S/N) than SANS, and is useful to detect both global and local conformational changes (Petoukhov and Svergun 2007; Svergun and Koch 2003; Tang et al. 2007, 2008a, b; Tang and Tsai 2008). Taken all together, one should consider SANS only when the answer cannot be provided by SAXS. Comparisons of some general properties of SANS versus SAXS are listed in Table 1, and more detailed information on theoretical perspectives and the studies of SAXS and SANS on biological systems can be found in further comprehensive reviews (Koch et al. 2003; Petoukhov and Svergun 2007; Svergun and Koch 2003; Vachette et al. 2003).

Dynamic light scattering

When light hits a homogenous, isotropic spherical particle in solution, the light scatters in all directions if the size of the particle (i.e., the scattering sphere) is (much) smaller than the wavelength of light. This phenomenon is called Rayleigh scattering (first quantitatively expressed by Lord Rayleigh in 1871) (Hoeppe and Stewart 2007). The Rayleigh approximation is expressed in Eq. 2:

$$I = I_o \frac{1 + \cos^2\theta}{2R^2} \left(\frac{2\pi}{\lambda}\right)^4 \left(\frac{n^2 - 1}{n^2 + 2}\right)^2 \left(\frac{d}{2}\right)^6 \quad (2)$$

where I and I_o are scattered and incident beam intensity, respectively, λ is the incident beam wavelength, θ is the scattering angle, n is the refractive index of the particle, R is the distance between the particle and the observing point, and d is the diameter of the particle (Bohren and Huffman 1983). As I (intensity of light scattered) is proportional to d^6 (d is the particle diameter), larger particles will contribute to (much) stronger scattered light intensity, and dynamic light scattering (DLS) is designed to measure the size (ranging from sub-nanometer to low micrometer, typically sub-micrometer region), diffusion coefficient, viscosity, and molecular weight of particles (Berne and Pecora 2000; Pecora 1983). SANS and SAXS are coherent elastic scattering methods, and DLS, also known as photon correlation spectroscopy (PCS), is a coherent quasi-elastic light scattering technique. While neutron and X-ray scattering probes the statistical ensemble of the microscopic structures in the sample, DLS measures the time dependence of the scattered light intensity from a very small area of solution (Berne and Pecora 1974). The fluctuations in the scattered light intensity are related to the diffusion rate of particles in and out of the area being monitored. Particles in the solution are constantly moving around, and the scattering intensity fluctuates due to the random thermal (Brownian) motion (or so called "random walk"), which is the random collision of particles (solutes) with surrounding solvent molecules (Brown 1828).

If the particles in Brownian motion are illuminated with a coherent and monochromatic light source, such as a laser, the intensity of the scattered light fluctuation is proportional to the size of the particles. Smaller (or larger) particles move faster (or slower) and have quick (or slow) fluctuations. Analysis of the scattering intensity fluctuations reflects the velocity of the Brownian motion, and the particle size (i.e., the average hydrodynamic diameter, d(H)) can be then obtained from the velocity using the Stokes–Einstein equation ($d(\mathrm{H}) = k_B T/3\pi\eta d_o$, where k_B is the Boltzmann constant, T is the absolute temperature, η is the viscosity of the solution, and d_o is the translational diffusion coefficient of the particle) (Hansen and McDonald 1986). Also, certain correlation factors, such as the refractive index of particles in the solution, are sometimes required to be optimized for calculation of the light scattering intensity and analyses of the DLS data (see Eq. 2). Moreover, the particle polydispersity can be estimated by the polydispersity index (PDI), a measurement of the distribution of molecular mass in a given sample. The PDI value is calculated from the width of the intensity size-

distribution profile (a plot of the relative light intensity scattered by particles versus size). The greater the sample polydispersity (or mono-dispersity), the larger (or smaller) the PDI value is. Also, when the size of biomolecules is probed by DLS, the global conformational change of biomolecules and/or an increase or decrease in the size of biomolecules will affect their diffusion rates. DLS is thus a very sensitive tool to monitor changes in size and shape of biomolecules.

While SANS (or SAXS) and DLS have been used to probe the size of particles, the particle size is estimated by SANS (or SAXS) through neutrons (or X-rays) interacting with nuclei (or electrons) in the molecules, and by DLS depending on how molecules diffuse within the medium. Further, the hydrodynamic diameter obtained by DLS is the diameter of a hypothetical solid sphere that travels with the same diffusion coefficient as the observed particles. Assuming that the effects of particle deformation, dynamic solvent penetration, solvent–particle interactions, and inter-particle interactions can be ignored, d(H) provides an average size that should fall somewhere in between the maximum and minimum dimensions of the particle. Thus, the size information of biomolecules determined by SANS (or SAXS) versus DLS may be different. Moreover, as the average hydrodynamic diameter of proteins and biological molecules estimated by DLS depends on their shape (conformation) and molecular mass, and their diffusion is also affected by water molecules bound or entrapped by the biomolecules as well as the ionic strength of the medium, the hydrodynamic size of biomolecules estimated by DLS may sometimes differ from the size determined by atomic-resolution approaches, such as NMR and crystallography.

Applications of SANS, SAXS, and DLS

One can perform biochemistry in situ during SANS, SAXS, and DLS measurements, but should note that because of the (very) low resolution, the scattering data can be appropriately interpreted only when (a) the biochemistry of the system is well understood and (b) the system is well behaved. What both SAXS and SANS can inform us about is the "envelope" of the molecules, in which the "size and global shape" of molecules are reported by the scattering data in the low q range and higher resolution of the shape can be determined from the scattering data in the mid- and high-q region (particularly for SAXS measurements) (Putnam et al. 2007). Thus, more structural information can be acquired from SAXS and SANS than from DLS. Alternatively, DLS can readily probe structural information of the aggregation (inter-particle interference)-prone biomolecules. Further, DLS requires a much shorter time (within 1–2 min) than SANS measurements (minutes to hours) for probing the particle size and other structural information, so one can probe the near real-time structural information of particles and biomolecules with minimal sample preparation (see below). Combinations of SANS and DLS have been used to characterize self-assembled polymers and the structural features of biomolecules and protein (or polymer)–surfactant complexes (Borsali et al. 1998; Chodankar et al. 2007; Hanson et al. 2001; Inomoto et al. 2009; Mears et al. 1998; Okabe et al. 2004; Romer et al. 2003; Yajima et al. 1998). In summary, SANS has great potential to assist structural investigation for biological systems that will not crystallize and/or have little hope of acquiring atomic-resolution structures (some examples are illustrated below). Additional structure–function information can be obtained from SANS when high-resolution structural data are available. Whether the scattering data is informative and the interpretation from scattering data is valid is highly dependent on sample preparation and other knowledge in well-defined systems.

Recent SANS and DLS studies on the photosystems of green and purple phototrophic bacteria

Most of the photosystems, including light-harvesting (or antenna) complexes (LHCs) and reaction centers (RCs), in phototrophs are membrane-bound protein–pigment complexes that are required to be reconstituted with detergents once extracted from the cell membrane. In contrast to water-soluble proteins, crystal structures reported for transmembrane proteins are much fewer in number principally due to the difficulty of obtaining well-ordered crystals. In this regard, SANS can be an alternative approach, in addition to cryo-EM and other advanced microscopic methods, for acquiring low-resolution structural information of the photosystems in solution. Together with SAXS, SANS has been employed to investigate several photosystems of various phototrophs over the years. Tiede and Thiyagarajan have reported SANS studies for photosynthetic supramolecular assembly prior to 1996 (Tiede and Thiyagarajan 1996), and several papers have been reported for the photosystems of oxygenic phototrophs (Cardoso et al. 2009) and of purple anoxygenic bacteria (Tiede et al. 2000; Wang et al. 2003). Without duplicating other reports on the subject, we review herein recent SANS and DLS studies from us and other researchers on green and purple phototrophic bacteria.

As illustrated above, the best structural information for proteins in the protein–detergent complex can be acquired by SANS if the protein can be deuterated. Alternatively, since different contrast points are reported for proteins and lipids (or detergents) in D_2O, scattering length density matching by SANS can provide structural information of the protein–

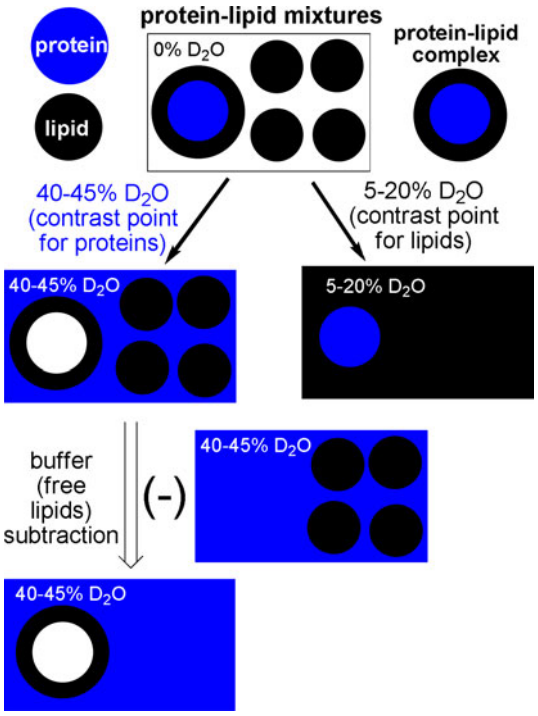

Fig. 2 Structural information for protein and bound lipids of protein–lipid complexes acquired by contrast variation in SANS

detergent complex without isotope labeling. As contrast points are distinct for proteins (40–45% D_2O) and lipids/detergents (e.g., lauryldimethylamine-*N*-oxide (LDAO), 5% D_2O; *n*-octyl-β-D-glucopyranoside (βOG), 17% D_2O), the overall size and low-resolution structural information for proteins and detergent-solubilized complexes in protein-pigment complexes, such as LHCs and RCs, can be obtained by changing D_2O/H_2O ratios (Fig. 2). Nevertheless, since lipids, photosynthetic pigments (e.g., (bacterio)chlorophylls and carotenoids) and cofactors in protein–pigments complexes have similar contrast points, contrast variation may or may not be able to provide structural insights of small molecules in detergent-reconstituted protein–pigment complexes.

Studies on the purple phototrophic bacteria

Conducing SANS in different ratios of D_2O buffer for contrast variation, we have recently probed the size of the RC in RC–LDAO mixtures and the LH2 (i.e., the B800-850 complex) in LH2–LDAO mixtures from the purple phototrophic bacterium *Rhodobacter sphaeroides* (Tang et al. 2010). During the light-harvesting process, purple bacteria first absorb photons by the LH2, and the excited energy is transferred to the light-harvesting LH1 core complex, and then funneled into the RC (Blankenship 2002; Hunter et al. 2008) (Fig. 3a). Structure and function of light-harvesting antenna complexes and RC in purple bacteria have been investigated in-depth (Cogdell et al. 2004a, b). The LH2 has been shown as an $(\alpha\beta)_9$ oligomer in the crystal structures (Papiz et al. 2003), while smaller or larger LH2 particles have also been reported (Savage et al. 1996). It remains to be understood why different oligomeric states of the LH2 are formed. Our recent SANS measurements (Tang et al. 2010) suggested that the solution conformation and crystal structure of the LH2 from purple bacteria are similar, implying that in our studies most of the LH2 complexes contain nine subunits of the $\alpha\beta$-heterodimer. As shown in Fig. 4a, the $P(r)$ distribution of LH2 in 45% D_2O suggests that LDAO detergent molecules occupy the central cavity (increased frequency of the shorter pair distance) as well as the surrounding LH2 barrel (increased frequency of the longer pair distance). Further, the values of the radius of gyration (R_g) and the longest distance within the particle (D_{max}) for LH2–LDAO mixtures in 100% D_2O are larger than the values calculated from the crystal structure of LH2 (PDB ID 1NKZ) (Table 2), also indicating that LDAO detergent molecules occupy the periphery of LH2 (Tang et al. 2010).

Studies on the green phototrophic bacterium *Cfl. aurantiacus*

Recently, we have used SANS to probe the size and shape of the photosystems of the filamentous anoxygenic phototrophic (FAP) bacterium *Chloroflexus aurantiacus*, which can perform photosynthesis in extremely low-light environments (Tang et al. 2010, 2011). Both FAPs and purple bacteria have a type II (quinone type) RC, whereas different LHCs are employed for transferring excited energy to the RC. The chlorosomes is the peripheral LHC and the B808-866-RC complex is the core complex of *Cfl. aurantiacus*, whereas the LH2 is the peripheral LHC and the LH1–RC complex is the core complex of purple bacteria (Fig. 3). While atomic-resolution structures for the photosystems of several purple bacteria have been revealed by X-ray crystallography or neutron diffraction (Allen et al. 1987; Arnoux et al. 1989; Deisenhofer et al. 1985, 1995; Deisenhofer and Michel 1989a, b; Isaacs et al. 1995; Papiz et al. 2003; Roszak et al. 2003, 2004; Roth et al. 1991; Stowell et al. 1997), the atomic-resolution structures for the LHCs (e.g., chlorosomes and the light-harvesting B808-866 core complex) and RC of *Cfl. aurantiacus* have not yet been reported.

The light-harvesting B808-866 core complex and the reaction center

The integral membrane light-harvesting B808-866 complex has somewhat unusual properties relative to the LHCs of

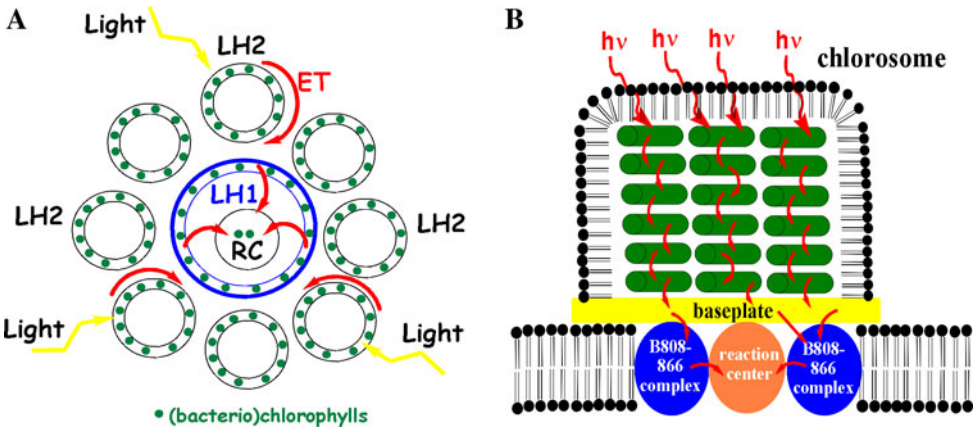

Fig. 3 Schematic representation of the proposed excited energy transfer in the photosystems of purple bacteria (**a**) versus *Cfl. aurantiacus* (**b**). During light-harvesting, purple bacteria (or *Cfl. aurantiacus*) first absorb photons by the LH2 (or the chlorosomes and then to the baseplate complex), and the excited energy is transferred to the light-harvesting LH1 core complex (or the light-harvesting B808-866 core complex), and then funneled into the RC

purple bacteria: its spectral features are similar to the LH2, while its sequence is more akin to the LH1 (i.e., the B880 complex) (Wechsler et al. 1987). It has been proposed that the B808-866 complex functions similarly to the purple bacterial LH1, while the hypothesis has not been fully examined. Using contrast variation for measuring SANS of the B808-866-βOG mixtures in various D_2O ratios, our studies indicate that the size of the B808-866 complex is $\sim$10% larger than that of the LH1 from purple bacteria (Table 2). Also, the $P(r)$ profile of B808-866-βOG mixtures in 17% D_2O has the reduced frequency of shorter pair distance (Fig. 4b), suggesting that the B808-866 complex, like the LH1 in purple bacteria, has a hollow structure. The value of D_{max} of B808-866-βOG mixtures in 100% D_2O is larger than the value in 17% D_2O (Table 2), indicating that βOG detergent molecules wrap around the B808-866 complex. Further, the $P(r)$ profile of B808-866-βOG mixtures in 100% D_2O shows the increased frequency of shorter pair distance (Fig. 4b), implying βOG molecules also filling up the central hollow space. The slightly larger size of the B808-866 complex than the LH1 may be correlated to two groups of bacteriochlorophylls (BChls) (B808 and B866) in the B808-866 complex versus one group of BChls (B880) in LH1, and the binding of the second group of BChls may change the protein scaffold in the B808-866 complex. Meanwhile, the overall size of B808-866-βOG mixtures was also examined by DLS, and only one population of B808-866 complex was detected in the size-distribution profile (Tang et al. 2010).

Further, the RC–LH core complex in *Roseiflexus castenholzii*, which is a FAP bacterium and closely related organism to *Cfl. aurantiacus*, was also reported to be arranged similarly as the RC–LH1 core complex (Collins et al. 2010). The average diameter of the LH in the RC–LH core complex (130 $\pm$ 10 Å) determined by electron microscopy is very similar to the ring diameter of the B808-866 complex in *Cfl. aurantiacus* (132 $\pm$ 5 Å) estimated by our SANS studies (Tang et al. 2010). Again, although the structural insights provided by SANS are limited for trans-membrane photosystems versus the information obtained from atomic-resolution structures, these studies show that useful information for the structure–function relationship of the photosystems can be acquired in the absence of high-resolution structures.

SANS measurements of the *Cfl. aurantiacus* RC in various D_2O ratios indicate that the size (both R_g and D_{max}) of the *Cfl. aurantiacus* RC is $\sim$20% smaller than that of the purple bacterial RC (Table 2), in agreement with the biochemical characterization that the *Cfl. aurantiacus* RC is simpler than the purple bacterial RC and only contains the L- and M-subunit, not the H-subunit (Pierson and Thornber 1983; Shiozawa et al. 1987). Also, the $P(r)$ profile of RC–LDAO mixtures in 100% D_2O (Fig. 4c) has the increased density toward the shorter distance and a rather narrow tail, implying a slightly elongated and cylindrical particle for the *Cfl. aurantiacus* RC and the *Rba. sphaeroides* RC. The conformation of the *Rba. sphaeroides* RC in solution suggested by SANS measurements is consistent with crystal structures of the purple bacterial RC (Roszak et al. 2003; Stowell et al. 1997). Together, our studies suggest that the B808-866 complex is wrapped around the RC, and that the B808-866-RC co-complex in *Cfl. aurantiacus* and the LH1–RC co-complex in purple bacteria are probably arranged similarly.

Chlorosomes

Green photosynthetic bacteria, including *Cfl. aurantiacus*, employ the chlorosomes as the peripheral light-harvesting antennas (Oostergetel et al. 2010). *Cfl. aurantiacus* usually lives in close proximity to cyanobacteria, thus in contrast to chlorosomes synthesized in the strictly anaerobic green sulfur bacteria, the *Cfl. aurantiacus* chlorosomes are not sensitive to redox regulation and not vulnerable to oxygen (Blankenship and Matsuura 2003). Chlorosomes are attached to the cytoplasmic membrane of the cell and encapsulated with a lipid monolayer, and are water-soluble

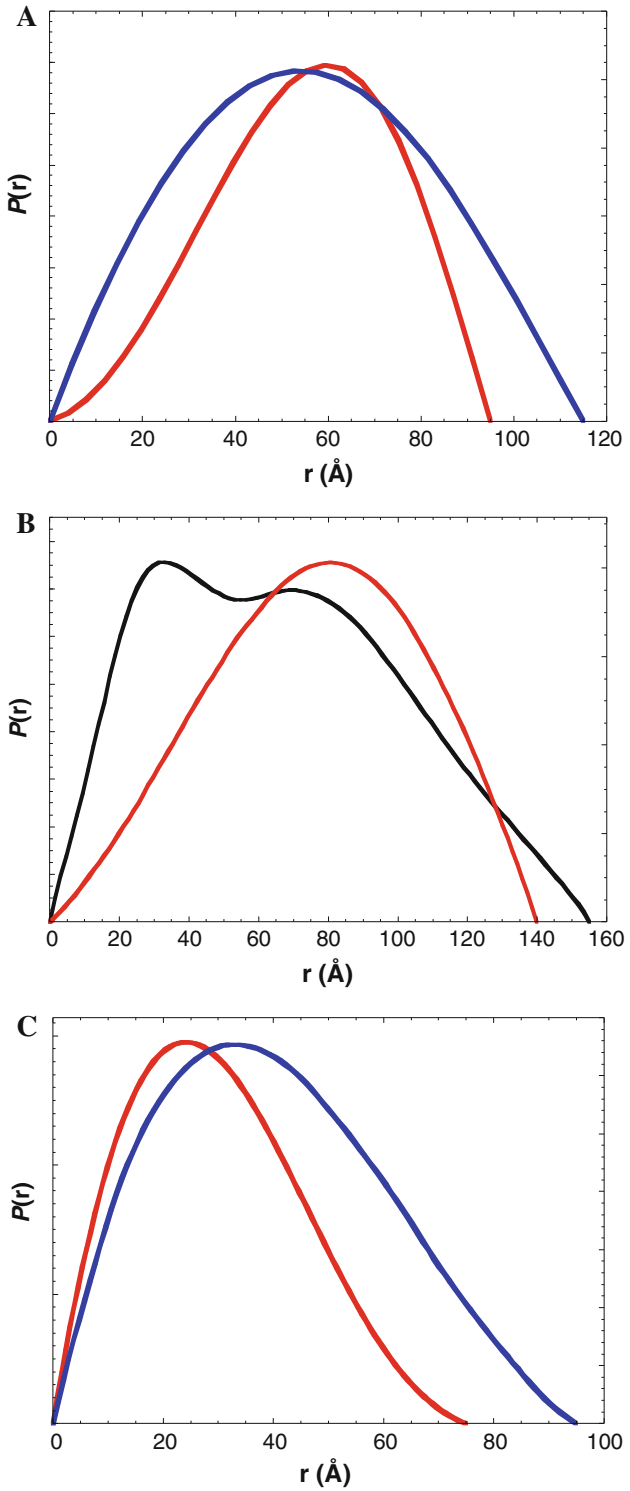

Fig. 4 The particle distance distribution function ($P(r)$) profiles of the photosystems in the purple bacterium *Rhodobacter sphaeroides* and in *Cfl. aurantiacus*. The *Rba. sphaeroides* LH2–LDAO mixtures in 45% (*blue curve*) and 10% D_2O (*red curve*) (**a**), B808-866-βOG mixtures in 100% (*black curve*) and 17% D_2O (*red curve*) (**b**), and RC–LDAO mixtures in 100% D_2O (RC in *Cfl. aurantiacus* (*red curve*) and *Rba. sphaeroides* (*blue curve*)) (**c**). The scattering profiles and data analyses were reported previously (Tang et al. 2010)

versus other membrane-bound LHCs that are required to be reconstituted by detergents. While proteins are essential for the scaffold of the protein-pigment LHCs, little protein is associated with chlorosomes, which is a pigment–pigment self-assembled complex, and the proteins are suggested to play only secondary roles. The size of chlorosomes is varied from various growth conditions, but the overall size of chlorosomes has been estimated to be within the nano-scale material range (Blankenship and Matsuura 2003). Altogether, these unique properties make chlorosomes a nice target for developing biohybrid solar cell nanodevices.

The detailed atomic level structures for chlorosomes are not yet available due to the very large size (estimated to be ~100 MDa effective molecular mass) (Tang et al. manuscript in preparations) and long-range disorder (Tang et al. 2011). The overall size of chlorosomes has been investigated by DLS (Modesto-Lopez et al. 2010; Montaño et al. 2003; Sridharan et al. 2008), although the reported hydrodynamic diameter of chlorosomes in the literature has significant variation, which could be related to different growth conditions and sample preparation methods. Note that chlorosomes are non-spherical particles, the average hydrodynamic diameter of particles determined by DLS assumes that particles are spherical in shape, as indicated in the brief introduction of DLS above (see "Dynamic light scattering" section) and in the literature.

Using SANS and other biophysical approaches, Worcester et al. reported that isolated chlorosomal BChls formed cylindrical micelles and estimated the cross-sectional radius of the free BChls self-assemblies (Worcester et al. 1986, 1989), and Wang et al. investigated the structural information of dimeric BChls (Wang et al. 1997). Further, SAXS, which can provide much higher S/N than SANS, has also recently been employed to probe the arrangement of BChls in chlorosomes (Pšencík et al. 2009, 2004). SANS is known to be a useful technique to acquire structural information of nano-particles like chlorosomes, because a longer wavelength can be chosen for neutron scattering. We have recently used a neutron wavelength of 18 Å to probe the size and shape of the *Cfl. aurantiacus* chlorosomes and a wavelength of 6 Å to investigate other LHCs. Our studies indicated that the *Cfl. aurantiacus* chlorosomes in solution are rod (or cylinder)-like particles with the cross-sectional radius ~20 nm (Tang et al. 2010, 2011), in agreement with previous EM studies (Martinez-Planells et al. 2002; Oelze and Golecki 1995; Sridharan et al. 2008; Staehelin et al. 1978).

A lamellar peak at $q = \sim 0.2$ Å^{-1} corresponding to the spacing (d) ~3.2 nm between crystal planes ($d = 2\pi/q$) was reported by SAXS on chlorosomes from *Cfl. aurantiacus* (Pšencík et al. 2009) and from the green sulfur bacteria (Pšencík et al. 2004). Note that the lamellar peak reported by SAXS (Fig. 5a) cannot be identified by the

Table 2 The structural parameters for the photosystems of purple bacteria and *Cfl. aurantiacus* obtained by SANS measurements and estimated by the atomic-resolution structures[a,b]

	R_g(Guinier)	R_g (CRYSON)	R_c (modified Guinier)	R_g (GNOM)	D_{max} (GNOM)
Purple bacteria					
The LH2 from *Rba. sphaeroides* (in LH2-LDAO mixtures)	30 ± 14 Å (10% D_2O)			35 ± 5 Å (10% D_2O)	95 ± 5 Å (10% D_2O)
	36 ± 2 Å (100% D_2O)			37 ± 1 Å (100% D_2O)	115 ± 3 Å (100% D_2O)
The LH2 from *Rps. acidophila* (PDB ID: 1NKZ)		33.2 Å		34 ± 1 Å	90 ± 2 Å
The LH1 from *Rps. palustris* (PDB ID: 1PYH)		47.2 Å		47 ± 0.4 Å	124 ± 2 Å
The RC from *Rba. sphaeroides* (in RC-LDAO mixtures)	38 ± 2 Å (100% D_2O)			35 ± 1 Å (100% D_2O)	95 ± 5 Å (100% D_2O)
The RC from *Rba. sphaeroides* (PDB ID: 1AIJ)		29.4 Å		30 ± 0.4 Å	85 ± 2 Å
Cfl. aurantiacus					
Chlorosomes (in 20 mM Tris–HCl at 100% D_2O)			200 ± 8 Å[b]	200 ± 4 Å[b]	825 ± 10 Å[b]
The B808-866 complex (in B808-866-βOG mixtures)	52 ± 6 Å (17% D_2O)			50 ± 2 Å (17% D_2O)	140 ± 5 Å (17% D_2O)
	60 ± 1 Å (100% D_2O)			56 ± 1 Å (100% D_2O)	155 ± 5 Å (100% D_2O)
RC (in RC–LDAO mixtures)	26 ± 10 Å (5% D_2O)			23 ± 5 Å (17% D_2O)	65 ± 5 Å (17% D_2O)
	32 ± 1 Å (100% D_2O)			28 ± 1 Å (100% D_2O)	75 ± 5 Å (100% D_2O)

[a] The reported values are from the previous studies (Tang et al. 2010)

[b] The reported values are from a recent paper (Tang et al. 2011)

SANS measurements (Tang et al. 2010) (Fig. 5b), and we hypothesize that the difference may be correlated to (a) the scattering contrast of atoms in neutrons versus in X-rays, and/or (b) much lower neutron flux leading to weaker structural features in the higher q region of the SANS profile (the lamellar peak at $q \sim 0.2$ Å^{-1} was reported by SAXS). Further experiments on SANS, SAXS and other biophysical approaches are required to elucidate the arrangement of BChls in chlorosomes.

The recent studies by DLS and SANS suggest that chlorosomes are highly heat-tolerant and remain intact up to 75°C (Tang et al. 2011). The thermal stability of chlorosomes is remarkable, compared to the thermal stability of most proteins, even if one considers that *Cfl. aurantiacus* is a moderately thermophilic filamentous bacterium and is cultured at 52–55°C (Hanada and Pierson 2006; Pierson and Castenholz 1974). Additionally, as indicated in the intensity size-distribution profile (Fig. 6a), larger chlorosomal particles (aggregates) are formed in high ionic strength, in contrast to high salt reducing the non-specific intermolecular attractive interactions reported in many biological systems. Further, SANS measurements indicate no changes in the mid-q ($0.0064 < q < 0.142$ Å^{-1}) to high-q ($0.026 < q < 0.64$ Å^{-1}) data range, and identical UV–vis and fluorescence emission spectra, as well as the identical Q_y band in circular dichroism (CD) spectra. These results suggest that there is no disruption of the internal pigment assembly in the salt-induced chlorosomal aggregates (Tang et al. 2011). Compared to other photosystems, the high phosphate buffer concentration required for the assembly and stability of phycobilisomes has been known for decades (Katoh 1988), whereas the temperature and ionic strength effects of chlorosomes have not been reported previously prior to our recent studies (Tang et al. 2011).

Further, DLS has been used to follow the stability of chlorosomes over time against pH and various salts, and found that the formation of large particles is a time-dependent process. Figure 6b shows some time-dependent size measurements of chlorosomes in different concentrations of NaCl (0–500 mM), and Fig. 6c illustrates the hydrodynamic diameter versus time profile of chlorosomes in 20 mM Tris–HCl buffer with or without various 150 mM salt included. The salts accelerate the large aggregate formation faster in divalent metal ions than in monovalent metal ions, $Ca^{2+} > Mg^{2+} \gg Na^{+} > K^{+}$. Our results also show that chloride has more effect on aggregation than bromide, nitrate and sulfate (Tang et al. 2011),

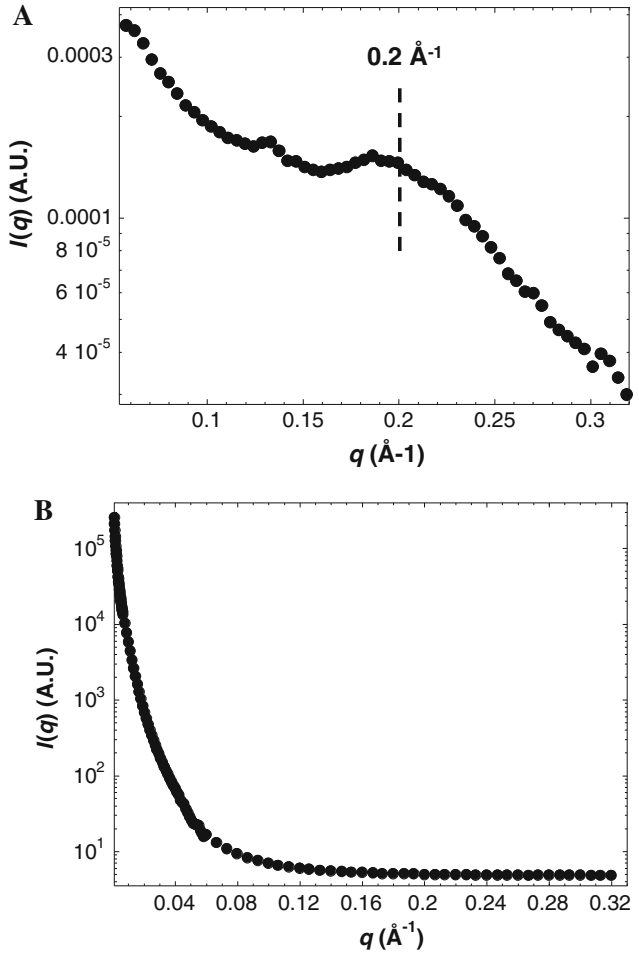

Fig. 5 The reported SAXS (**a**) versus SANS (**b**) profiles for the *Cfl. aurantiacus* chlorosomes. The SAXS data in **a** is from Dr. Jakub Pšenčík of Charles University, Czech Republic (unpublished results). The SANS data in **b** were collected in 20 mM Tris–HCl buffer (at pH 8.0) in 100% D_2O. The SAXS data in $0.05 < q < 0.33$ Å^{-1} (**a**) and the SANS data in $0.0009 < q < 0.33$ Å^{-1} (**b**) are shown

consistent with the trend predicted by the Hofmeister interactions/effects (Baldwin 1996; Lyklema 2009; Zhang and Cremer 2010). We propose that the aggregation of chlorosomes is due to high salt conditions that minimize intermolecular repulsive interactions (Tang et al. 2011).

These near real-time size measurements of chlorosomes cannot be followed by SANS, which requires longer measurement time (minutes to hours) to generate useful information. Alternatively, SAXS can be used to follow time-dependent reactions with an appropriate experimental setup and more structural features can be obtained, whereas synchrotron radiation sources, which are not readily accessible for many laboratories, are required to obtain the real-time structural information of chlorosomes. Additionally, higher sample concentrations are usually required for SAXS than for DLS, and the samples cannot be re-used after SAXS measurements due to radiation damage. Taken

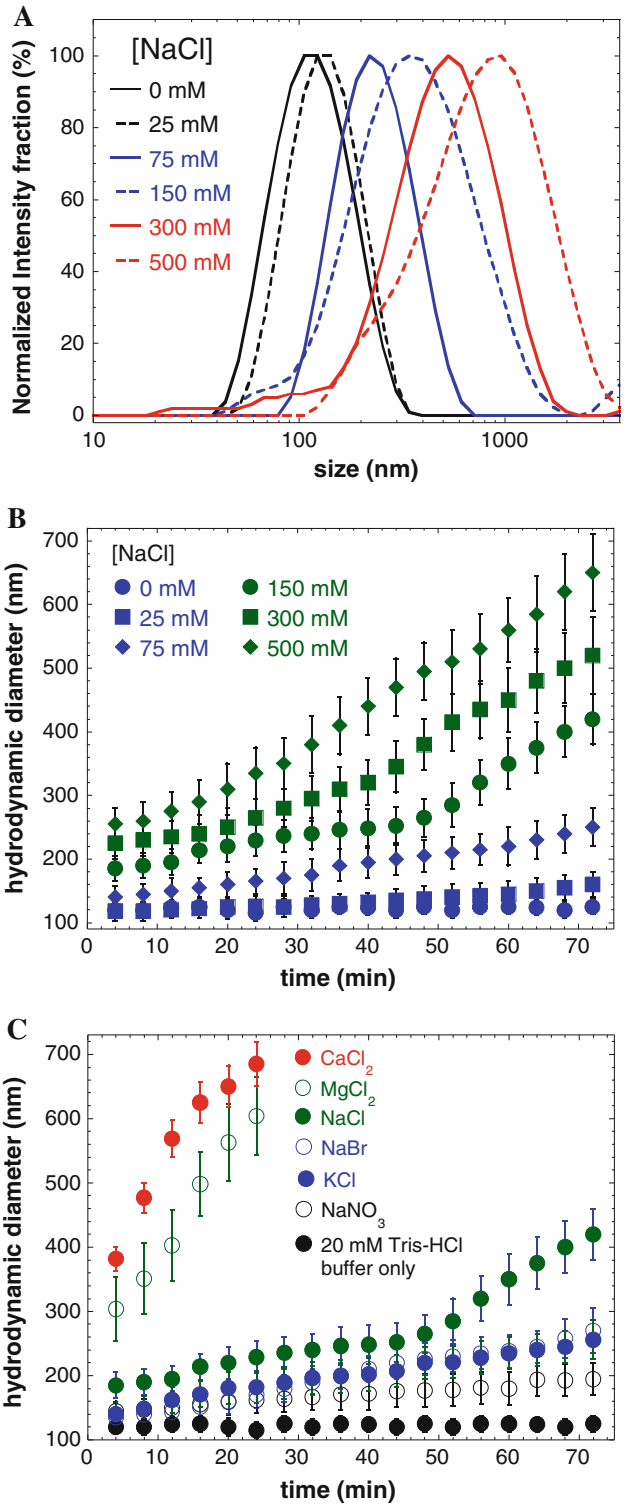

Fig. 6 DLS measurements of the *Cfl. aurantiacus* chlorosomes in various ionic strength environments. The intensity size-distribution profile of chlorosomes incubated in various concentrations of NaCl for 60 min (**a**), time-dependent size measurements of chlorosomes in 0, 25, 75, 150, 300, and 500 mM NaCl (**b**), and the hydrodynamic diameter versus time profile of chromosomes in 20 mM Tris–HCl buffer with or without 150 mM various salt included (**c**)

together, DLS, in addition to being easily accessible, can readily investigate size information of chlorosomes with minimal sample preparation and probe the near real-time information and physicochemical properties of chlorosomes without incurring radiation damage.

Acknowledgments The authors thank Dr. Volker S. Urban at Oak Ridge National Laboratory for assistance on SANS data collection and Dr. Pratim Biswas at the Department of Energy, Environmental and Chemical Engineering at Washington University on the work of the chlorosomes. We also thank Dr. Jakub Pšenčík of Charles University, Czech Republic for the unpublished results in Fig. 5A and helpful discussions on the types of information available from SAXS and SANS. This paper is based upon work supported as part of the Photosynthetic Antenna Research Center (PARC), an Energy Frontier Research Center funded by the U.S. Department of Energy, Office of Science, Office of Basic Energy Sciences under Award Number DE-SC 0001035.

References

Allen JP, Feher G, Yeates TO, Komiya H, Rees DC (1987) Structure of the reaction center from *Rhodobacter sphaeroides* R-26: the protein subunits. Proc Natl Acad Sci USA 84:6162–6166

Arnoux B, Ducruix A, Reiss-Husson F, Lutz M, Norris J, Schiffer M, Chang CH (1989) Structure of spheroidene in the photosynthetic reaction center from Y *Rhodobacter sphaeroides*. FEBS Lett 258:47–50

Baldwin RL (1996) How Hofmeister ion interactions affect protein stability. Biophys J 71:2056–2063

Berne BJ, Pecora R (1974) Laser light scattering from liquids. Ann Rev Phys Chem 25:233–253

Berne BJ, Pecora R (2000) Dynamic light scattering with applications to chemistry, biology and physics. Dover, New York

Blankenship RE (2002) Molecular mechanisms of photosynthesis. Blackwell Science Ltd, Oxford

Blankenship RE, Matsuura K (2003) Antenna complexes from green photosynthetic bacteria. In: Green BR, Parson WW (eds) Anoxygenic photosynthetic bacteria. Kluwer Academic Publishers, Dordrecht, pp 195–217

Bohren CF, Huffman D (1983) Absorption and scattering of light by small particles. Wiley, New York

Borsali R, Nguyen H, Pecora R (1998) Small-angle neutron scattering and dynamic light scattering from a polyelectrolyte solution: DNA. Macromolecules 31:1548–1555

Brown R (1828) A brief account of microscopical observations made in the months of June, July and August, 1827, on the particles contained in the pollen of plants; and on the general existence of active molecules in organic and inorganic bodies. Philos Mag 4:161–173

Cardoso MB, Smolensky D, Heller WT, O'Neill H (2009) Insight into the structure of light-harvesting complex II and its stabilization in detergent solution. J Phys Chem B 113:16377–16383

Chadwick J (1932a) The existence of a neutron. Proc R Soc A 136:692–708

Chadwick J (1932b) Possible existence of a neutron. Nature 129:312

Chodankar S, Aswal VK, Kohlbrecher J, Vavrin R, Wagh AG (2007) Surfactant-induced protein unfolding as studied by small-angle neutron scattering and dynamic light scattering. J Phys 19:326102

Cogdell RJ, Gardiner AT, Roszak AW, Law CJ, Southall J, Isaacs NW (2004a) Rings, ellipses and horseshoes: how purple bacteria harvest solar energy. Photosynth Res 81:207–214

Cogdell RJ, Hashimoto H, Gardiner AT (2004b) Purple bacterial light-harvesting complexes: from dreams to structures. Photosynth Res 80:173–179

Collins AM, Qian P, Tang Q, Bocian DF, Hunter CN, Blankenship RE (2010) Light-harvesting antenna system from the phototrophic bacterium *Roseiflexus castenholzii*. Biochemistry 49:7524–7531

Crawford RK (1996) Gas detectors for neutrons. J Neutron Res 4:97–107

Deisenhofer J, Michel H (1989a) Nobel lecture. The photosynthetic reaction centre from the purple bacterium *Rhodopseudomonas viridis*. EMBO J 8:2149–2170

Deisenhofer J, Michel H (1989b) The photosynthetic reaction center from the purple bacterium *Rhodopseudomonas viridis*. Science 245:1463–1473

Deisenhofer J, Epp O, Miki K, Huber R, Michel H (1985) Structure of the protein subunits in the photosynthetic reaction center of *Rhodopseudomonas viridis* at 3 Å resolution. Nature 318:618–624

Deisenhofer J, Epp O, Sinning I, Michel H (1995) Crystallographic refinement at 2.3 Å resolution and refined model of the photosynthetic reaction centre from *Rhodopseudomonas viridis*. J Mol Biol 246:429–457

Duderstadt JJ, Hamilton LJ (1976) Nuclear reactor analysis. Wiley, New York

Feigin LA, Svergun DI (1987) Structure analysis by small-angle X-ray and neutron scattering. Plenum Press, New York

Gabel F, Bicout D, Lehnert U, Tehei M, Weik M, Zaccai G (2002) Protein dynamics studied by neutron scattering. Q Rev Biophys 35:327–367

Glatter O (1977) New method for evaluation of small-angle scattering data. J Appl Cryst 10:415–421

Hanada S, Pierson BK (2006) The family chloroflexaceae. The Prokaryotes, vol 7, 3rd edn. Springer, New York, pp 815–842

Hansen JP, McDonald IR (1986) Theory of simple liquids. Academic Press, New York

Hanson ET, Borsali R, Pecora R (2001) Dynamic light scattering and small-angle neutron scattering studies of ternary rod/coil/solvent systems. Macromolecules 34:2208–2219

Hoeppe G, Stewart J (2007) Why the sky is blue: discovering the color of life. Princeton University Press, Princeton

Hunter CN, Daldal F, Thurnauer MC, Beatty JT (2008) The purple phototrophic bacteria. In: Hunter CN, Daldal F, Thurnauer MC, Beatty JT (eds) Advances in photosynthesis and respiration, vol 28. Springer, Dordrecht, The Netherlands

Inomoto N, Osaka N, Suzuki T, Hasegawa U, Ozawa Y, Endo H, Akiyoshi K, Shibayama M (2009) Interaction of nanogel with cyclodextrin or protein: study by dynamic light scattering and small-angle neutron scattering. Polymer 50:541–546

Isaacs NW, Cogdell RJ, Freer AA, Prince SM (1995) Light-harvesting mechanisms in purple photosynthetic bacteria. Curr Opin Struct Biol 5:794–797

Jacrot B (1976) Study of biological structures by neutron-scattering from solution. Rep Prog Phys 39:911–953

Katoh T (1988) Phycobilisome stability. Meth Enzymol 167:313–318

Koch MH, Vachette P, Svergun DI (2003) Small-angle scattering: a view on the properties, structures and structural changes of biological macromolecules in solution. Q Rev Biophys 36:147–227

Lyklema J (2009) Simple Hofmeister series. Chem Phys Lett 467:217–222

Martinez-Planells A, Arellano JB, Borrego CM, Lopez-Iglesias C, Gich F, Garcia-Gil J (2002) Determination of the topography and biometry of chlorosomes by atomic force microscopy. Photosynth Res 71:83–90

Mears SJ, Cosgrove T, Obey T, Thompson L, Howell I (1998) Dynamic light scattering and small-angle neutron scattering studies on the poly(ethylene oxide)/sodium dodecyl sulfate/polystyrene latex system. Langmuir 14:4997–5003

Modesto-Lopez LB, Thimsen EJ, Collins AM, Blankenship RE, Biswas P (2010) Electrospray-assisted characterization and deposition of chlorosomes to fabricate a biomimetic light-harvesting device. Energy Environ Sci 3:216–222

Montaño GA, Bowen BP, LaBelle JT, Woodbury NW, Pizziconi VB, Blankenship RE (2003) Characterization of *Chlorobium tepidum* chlorosomes: a calculation of bacteriochlorophyll *c* per chlorosome and oligomer modeling. Biophys J 85:2560–2565

Moore PB (1980) Small-angle scattering. Information content and error analysis. J Appl Cryst 13:168–175

Oelze J, Golecki JR (1995) Membranes and chlorosomes of green bacteria: structure, composition and development. In: Blankenship RE, Madigan MT, Bauer CE (eds) Anoxygenic photosynthetic bacteria. Kluwer Academic Publishers, Dordrecht, The Netherlands, pp 259–278

Okabe S, Ando K, Hanabusa K, Shibayama M (2004) Dynamic light scattering and small-angle neutron scattering studies on organogels formed with a gelator. J Polym Sci A 42:1841–1848

Oostergetel GT, van Amerongen H, Boekema EJ (2010) The chlorosome: a prototype for efficient light harvesting in photosynthesis. Photosynth Res 104:245–255

Papiz MZ, Prince SM, Howard T, Cogdell RJ, Isaacs NW (2003) The structure and thermal motion of the B800-850 LH2 complex from Rps. acidophila at 2.0 Å resolution and 100 K: new structural features and functionally relevant motions. J Mol Biol 326:1523–1538

Pecora R (1983) Quasi-elastic light scattering of macromolecules and particles in solution and suspension. In: Dahneke BE (ed) Measurement of suspended particles by quasi-elastic light scattering. Wiley, New York, pp 3–30

Petoukhov MV, Svergun DI (2007) Analysis of X-ray and neutron scattering from biomacromolecular solutions. Curr Opin Struct Biol 17:562–571

Pierson BK, Castenholz RW (1974) A phototrophic gliding filamentous bacterium of hot springs, *Chloroflexus aurantiacus*, gen. and sp. nov. Arch Microbiol 100:5–24

Pierson BK, Thornber JP (1983) Isolation and spectral characterization of photochemical reaction centers from the thermophilic green bacterium *Chloroflexus aurantiacus* strain J-10-f1. Proc Natl Acad Sci USA 80:80–84

Price DL, Skold K (1986) Introduction to neutron scattering. In: Skold K, Price DL (eds) Methods of experimental physics, vol. 23 part a neutron scattering. Academic Press, Orlando, pp 1–97

Prince SM, Howard TD, Myles DA, Wilkinson C, Papiz MZ, Freer AA, Cogdell RJ, Isaacs NW (2003) Detergent structure in crystals of the integral membrane light-harvesting complex LH2 from *Rhodopseudomonas acidophila* strain 10050. J Mol Biol 326:307–315

Pšenčík J, Ikonen TP, Laurinmaki P, Merckel MC, Butcher SJ, Serimaa RE, Tuma R (2004) Lamellar organization of pigments in chlorosomes, the light harvesting complexes of green photosynthetic bacteria. Biophys J 87:1165–1172

Pšenčík J, Collins AM, Liljeroos L, Torkkeli M, Laurinmaki P, Ansink HM, Ikonen TP, Serimaa RE, Blankenship RE, Tuma R, Butcher SJ (2009) Structure of chlorosomes from the green filamentous bacterium *Chloroflexus aurantiacus*. J Bacteriol 191:6701–6708

Putnam CD, Hammel M, Hura GL, Tainer JA (2007) X-ray solution scattering (SAXS) combined with crystallography and computation: defining accurate macromolecular structures, conformations and assemblies in solution. Q Rev Biophys 40:191–285

Rauch H, Waschkowski W (2000) 6. Neutron scattering lengths. In: Schopper H (ed) Low energy neutrons and their interaction with nuclei and matter. Part 1. SpringerMaterials—the Landolt-Börnstein Database

Romer S, Urban C, Lobaskin V, Scheffold F, Stradner A, Kohlbrecher J, Schurtenberger P (2003) Simultaneous light and small-angle neutron scattering on aggregating concentrated colloidal suspensions. J Appl Cryst 36:1–6

Roszak AW, Howard TD, Southall J, Gardiner AT, Law CJ, Isaacs NW, Cogdell RJ (2003) Crystal structure of the RC–LH1 core complex from *Rhodopseudomonas palustris*. Science 302:1969–1972

Roszak AW, McKendrick K, Gardiner AT, Mitchell IA, Isaacs NW, Cogdell RJ, Hashimoto H, Frank HA (2004) Protein regulation of carotenoid binding; gatekeeper and locking amino acid residues in reaction centers of *Rhodobacter sphaeroides*. Structure 12:765–773

Roth M, Arnoux B, Ducruix A, Reiss-Husson F (1991) Structure of the detergent phase and protein-detergent interactions in crystals of the wild-type (strain Y) *Rhodobacter sphaeroides* photochemical reaction center. Biochemistry 30:9403–9413

Savage H, Cyrklaff M, Montoya G, Kuhlbrandt W, Sinning I (1996) Two-dimensional structure of light harvesting complex II (LHII) from the purple bacterium *Rhodovulum sulfidophilum* and comparison with LHII from *Rhodopseudomonas acidophila*. Structure 4:243–252

Sears VF (1986) Neutron scattering lengths and cross sections. In: Skoeld K, Price DL (eds) Methods of experimental physics, vol A23. New York, Academic Press, pp 521–550

Sears VF (1989) Neutron optics, neutron scattering in condensed matter, vol 3. Oxford University Press, New York

Shiozawa JA, Lottspeich F, Feick R (1987) The photochemical reaction center of *Chloroflexus aurantiacus* is composed of two structurally similar polypeptides. Eur J Biochem 167:595–600

Smith JC (1991) Protein dynamics: comparison of simulations with inelastic neutron scattering experiments. Q Rev Biophys 24:227–291

Squires GL (1997) Introduction to the theory of thermal neutron scattering. Dover Publications, New York

Sridharan A, Muthuswamy J, Labelle JT, Pizziconi VB (2008) Immobilization of functional light antenna structures derived from the filamentous green bacterium *Chloroflexus aurantiacus*. Langmuir 24:8078–8089

Staehelin LA, Golecki JR, Fuller RC, Drews G (1978) Visualization of the supramolecular architecture of chlorosomes (*Chlorobium* type vesicles) in freeze-fractured cells of *Chloroflexus aurantiacus*. Arch Microbiol 119:269–277

Stowell MH, McPhillips TM, Rees DC, Soltis SM, Abresch E, Feher G (1997) Light-induced structural changes in photosynthetic reaction center: implications for mechanism of electron–proton transfer. Science 276:812–816

Svergun DI, Koch MHJ (2003) Small-angle scattering studies of biological macromolecules in solution. Rep Prog Phys 66:1735–1782

Svergun DI, Semenyuk AV, Feigin LA (1988) Small-angle scattering data treatment by the regularization method. Acta Crystallogr A 44:244–250

Svergun DI, Pedersen JS, Serdyuk IN, Koch MH (1994) Solution scattering from 50S ribosomal subunit resolves inconsistency between electron microscopic models. Proc Natl Acad Sci USA 91:11826–11830

Tang KH, Tsai MD (2008) Structure and function of 2:1 DNA polymerase.DNA complexes. J Cell Physiol 216:315–320

Tang KH, Guo H, Yi W, Tsai MD, Wang PG (2007) Investigation of the conformational states of Wzz and the Wzz.O-antigen

complex under near-physiological conditions. Biochemistry 46:11744–11752

Tang KH, Niebuhr M, Aulabaugh A, Tsai MD (2008a) Solution structures of 2:1 and 1:1 DNA polymerase–DNA complexes probed by ultracentrifugation and small-angle X-ray scattering. Nucleic Acids Res 36:849–860

Tang KH, Niebuhr M, Tung CS, Chan HC, Chou CC, Tsai MD (2008b) Mismatched dNTP incorporation by DNA polymerase beta does not proceed via globally different conformational pathways. Nucleic Acids Res 36:2948–2957

Tang KH, Urban VS, Wen J, Xin Y, Blankenship RE (2010) SANS investigation of the photosynthetic machinery of *Chloroflexus aurantiacus*. Biophys J 99:2398–2407

Tang KH, Zhu L, Urban VS, Collins AM, Biswas P, Blankenship RE (2011) Temperature and ionic strength effects on the light-harvesting antenna complex chlorosomes. Langmuir 27:4816–4828

Taylor A, Dunne M, Bennington S, Ansell S, Gardner I, Norreys P, Broome T, Findlay D, Nelmes R (2007) A route to the brightest possible neutron source? Science 315:1092–1095

Tiede DM, Thiyagarajan P (1996) Characterization of photosynthetic supramolecular assemblies using small angle neutron scattering. In: Amez J, Hoff A (eds) Biophysical techniques in photosynthesis, vol 3. Kluwer Academic Publication, Dordrecht, The Netherlands, pp 375–390

Tiede DM, Littrell K, Maronea PA, Zhanga R, Thiyagarajan P (2000) Solution structure of a biological bimolecular electron transfer complex: characterization of the photosynthetic reaction center-cytochrome c2 protein complex by small angle neutron scattering. J Appl Cryst 33:560–564

Vachette P, Koch MHJ, Svergun DI (2003) Looking behind the beamstop: X-ray solution scattering studies of structure and conformational changes of biological macromolecules. Macromol Crystallogr D 374:584–615

Wang ZY, Umetsu M, Yoza K, Kobayashi M, Imai M, Matsushita Y, Niimura N, Nozawa T (1997) A small-angle neutron scattering study on the small aggregates of bacteriochlorophylls in solutions. Biochim Biophys Acta 1320:73–82

Wang ZY, Muraoka Y, Nagao M, Shibayama M, Kobayashi M, Nozawa T (2003) Determination of the B820 subunit size of a bacterial core light-harvesting complex by small-angle neutron scattering. Biochemistry 42:11555–11560

Wechsler TD, Brunisholz RA, Frank G, Suter F, Zuber H (1987) The complete amino acid sequence of the antenna polypeptide B806-866-beta from the cytoplasmic membrane of the green bacterium *Chloroflexus aurantiacus*. FEBS Lett 210:189–194

Worcester DL, Michalski TJ, Katz JJ (1986) Small-angle neutron scattering studies of chlorophyll micelles: models for bacterial antenna chlorophyll. Proc Natl Acad Sci USA 83:3791–3795

Worcester DL, Michalski TJ, Tyson RL, Bowman MK, Katz JJ (1989) Structure, red-shifted absorption and electron-transport properties of specific aggregates of chlorophylls. Physica B 156:502–504

Yajima H, Yamamoto H, Nagaoka M, Nakazato K, Ishii T, Niimura N (1998) Small-angle neutron scattering and dynamic light scattering studies of N- and C-terminal fragments of ovotransferrin. Biochim Biophys Acta 1381:68–76

Zhang Y, Cremer PS (2010) Chemistry of Hofmeister anions and osmolytes. Annu Rev Phys Chem 61:63–83